Growth and post-annealing studies of Bi$_2$Sr$_{2-x}$La$_x$CuO$_{6+\delta}$ (0≤ x ≤1.00) single crystals

Huiqian Luo, Peng Cheng, Lei Fang, Hai-Hu Wen

National Laboratory for Superconductivity, Institute of Physics and
National Laboratory for Condensed Matter Physics, P. O. Box 603 Beijing, 100190,
P. R. China

E-mail: hhwen@aphy.iphy.ac.cn

Abstract. Bi$_2$Sr$_{2-x}$La$_x$CuO$_{6+\delta}$ (0≤ x ≤1.00) single crystals with high-quality have been grown successfully using the travelling-solvent floating-zone technique. The patterns of X-ray diffraction suggest high crystalline quality of the samples. After post-annealing in flowing oxygen at 600 ^{o}C, the crystals show sharp superconducting transitions revealed by AC susceptibility. The hole concentration p is deduced from superconducting transition temperature (T_c), which exhibits a linear relation with La doping level x. It ranges from the heavily overdoped regime ($p \approx 0.2$) to the extremely underdoped side ($p \approx 0.08$) where the superconductivity is absent. Comparing with the superconducting dome in Bi$_{2+x}$Sr$_{2-x}$CuO$_{6+\delta}$ system, the effects from out-of-plane disorders show up in our samples. Besides the La doping level x, the superconductivity is also sensitive to the content of oxygen which could be tuned by post-annealing method over the whole doping range. The post-annealing effects on T_c and p for each La doping level are studied, which give some insights on the different nature between overdoped and underdoped regime.

1. Introduction

The high temperature superconductivity (HTSC) in copper oxides is one of the most important issues in condensed matter physics. In hole doped cuprates, the antiferromagnetic Mott insulator at half filling will be gradually replaced by a novel metallic state when the hole concentration p increases [1]. The hole doping dependence of superconducting transition temperature (T_c) forms a superconducting dome in the phase diagram [2], which is one of the central challenges to explain the mechanism of HTSC.

The single-layered cuprate Bi$_2$Sr$_2$CuO$_{6+\delta}$ (Bi2201) is one of the well studied materials for the mechanism of HTSC due to its advantage of relative lower T_c. The coordination of Sr^{2+} ions located next to the apical oxygen, which is defined as the A-site, could be occupied by the ions of lanthanide (Ln^{3+}) and bismuth (Bi^{3+}). It generates a large family including Bi$_2$Sr$_{2-x}$Ln$_x$CuO$_{6+\delta}$ (Ln= La, Pr, Nd, Sm, Eu, Gd, etc.)

systems and $Bi_{2+x}Sr_{2-x}CuO_{6+\delta}$ (Bi-Bi2201) system [3]. The mismatch between the size of substituted ions introduces A-site disorders, which result in different T_c ranging from 30 K to 10 K at the optimal doping level in each system [4]. The $Bi_2Sr_{2-x}La_xCuO_{6+\delta}$ (La-Bi2201) system has the weakest influence of disorders and the highest T_c in this family, while the case in the $Bi_{2+x}Sr_{2-x}CuO_{6+\delta}$ system is in the opposite way. The relationship between the disorders and T_c gives more opportunities to access the central problems in the mechanism of HTSC [5, 6], and single crystals with high quality are highly desired for such investigations.

It was reported that the Bi2201 single crystals could be grown by the self-flux and KCl-solution-melt method [7, 8, 9, 10]. However, as far as we know, sizeable crystals with high homogeneity and less contamination could be obtained only through the optical travelling-solvent floating-zone (TSFZ) method [11, 12, 13]. We have successfully grown high-quality $Bi_{2+x}Sr_{2-x}CuO_{6+\delta}$ single crystals with highly dense doping levels in the underdoped regime. The characterizations show that our crystals have high crystalline quality and sharp superconducting transitions. The quick contraction of c-axis accompanied with the suppression of superconductivity suggests that more disorders are introduced by doping Bi^{3+} into the Sr-O plane [14].

Besides the ionic substitution in the out-of-plane, it is known that the hole concentration of cuprates also controlled by the oxygen content which could be tuned by post-annealing method. When a sample is annealed at a certain temperature and atmosphere, the activated oxygen atoms redistribute inside the sample. The holes on O sites in Cu-O plane will be added or removed through these processes, thus the superconductivity could be tuned sensitively. However, there are rare reports on the post-annealing effects over the whole doping range in La-Bi2201 system, and the detailed behaviors for post-annealing are not clear yet [15, 16].

In this paper, we report the successful growth of $Bi_2Sr_{2-x}La_xCuO_{6+\delta}$ single crystals with high quality by TSFZ method. The nominal composition of La doping level x varies from 0 to 1.00, and the hole concentration of our crystals ranges from the heavily overdoped regime to the extreme underdoped side where the superconductivity is absent. The post-annealing experiments have been extensively carried out on the samples at each La doping level at different temperatures in flowing oxygen. The post-annealing effects on p and T_c are studied, which give different insights between underdoped and overdoped regime.

2. Experiments

The $Bi_2Sr_{2-x}La_xCuO_{6+\delta}$ ($0\leq x \leq1.00$) single crystals were grown by the TSFZ technique. The starting materials were prepared by a standard solid state reaction method before the crystal growth. In order to eliminate the moisture, the powders of $SrCO_3$ (99.99%) were baked at 200 ^{o}C for more than 5 hours. And the powders of La_2O_3 (99.99 %) were calcined at 1000 ^{o}C for 10 hours to make sure that $La(OH)_3$ has decomposed completely. After the pre-processes, they were mixed with Bi_2O_3 (99.99

%) and CuO (99.5%) in the stoichiometric proportion (2-x) : x/2 : 1 : 1. The mixed powders were ground by hand in a dry agate mortar for about 4 hours, and then they were calcined in a crucible at 800 ^{o}C for 24 hours inside a muffle furnace. As soon as the product was cooled down to room temperature, it was crushed into powder then ground and calcined again. This procedure was repeated for four times to ensure the homogeneity of the starting material. Finally, the homogenous polycrystalline powder was pressed into a cylindrical rod of ϕ7 mm × 90 mm under hydrostatical pressure at ~70 MPa, then it was sintered in a vertical furnace at 850 ^{o}C for 36 hours in air. In order to get a feed rod with higher density and sufficient oxygen content, the premelting process was performed under oxygen pressure $P(O_2) = 2$ atm, and the moving speed of mirror stage was 30 mm/hr. After premelting, a homogeneous feed rod with ϕ6~7 mm in diameter and 60~80 mm in length was obtained.

Single crystal growth by the TSFZ method was performed with an optical floating-zone furnace which was produced by the *Crystal Systems Corporation*. A steep temperature gradient was obtained by using four 300 W halogen lamps as the heating sources. The crystal growth was done under an oxygen pressure with 2.0 ~ 3.5 atm in an enclosed quartz tube, and the flowing rate of O_2 was about 20 ~ 40 cc/min. The typical growth rate is about 0.50 mm/hr, and the rotation rate is 25.0 rpm for the upper shaft and 15.0 rpm for the lower shaft in opposite directions. The post-annealing was carried out under 1 atm flowing oxygen at a finite temperature for more than 150 hours at each step. At the end of treatment, the samples were quenched to room temperature in air.

The crystals cleaved from the as-grown ingots were selected carefully under polarization microscope, and then characterized by various techniques. The X-ray diffraction (XRD) measurements of the crystals were carried out by a *Mac- Science* MXP18A-HF equipment with $\theta - 2\theta$ scan to examine the crystalline quality of the samples. K_α radiation of Cu target was used, and the continuous scanning range of 2θ is from 5° to 80°. The composition of crystal was examined by the energy dispersive X-ray (EDX, Oxford-6566) analysis. The superconductivity of the crystals was characterized by AC susceptibility based on an *Oxford* cryogenic system Maglab-EXA-12 and a *Quantum Design* Magnetic Property Measurement System (MPMS). An alternating magnetic field $H = 0.1$ Oe was applied perpendicular to the *ab*-plane with a frequency f=333 Hz during the AC susceptibility measurement. The transition temperature of the samples was derived from AC susceptibility curve by the point where the real part of the susceptibility deviates from the flattened normal state part.
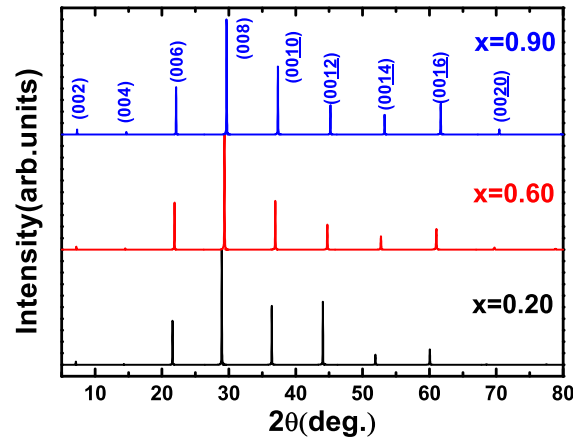
3. Results and discussion

3.1. Crystal growth and characterization

The crystal growth was performed under oxygen atmosphere enclosed by a quartz tube. In order to obtain high quality single crystals, the shape of melting-zone should be

Figure 1. (color online) One of the as-grown ingots with $x=$ 0.85 (below) and the cleaved ingot with $x=$ 0.40 (above).

Figure 2. (color online) Typical XRD patterns for cleaved single crystals with $x=$ 0.20, 0.60, 0.90. All peaks are very sharp with narrow FWHM around 0.1°.

rather stable during the growth. Thus the power of lamp, growth rate, rotation rate of shafts, pressure and flowing rate of oxygen should be carefully tuned. According to our experiences, the melting point of feed rod increases when more and more La_2O_3 is mixed into the staring material, and it is also related to the oxygen pressure. Two kinds of pressure were applied: $P(O_2)=$ 2.2 atm for underdoped samples with $0.40 \leq x \leq 1.00$ and $P(O_2)=$ 3.4 atm for overdoped samples with $0 \leq x \leq 0.30$, respectively. The other parameters are almost the same for each nominal composition during the growth. Large and plate-like single crystals could be obtained easily for $x \geq 0.70$. When x reduces to $0.40 \sim 0.60$, the cleaved as-grown crystals are lamellar. For the overdoped samples with $x < 0.40$, the growth of crystals are much more difficult. Since the viscosity of the melted compound is low during the growth, only needle-like crystals could be obtained for the compositions with $x=$ 0 and 0.05. One of the as-grown ingots with $x=$ 0.85 (below) and the cleaved ingot with $x=0.40$ (above) are shown in Figure 1. The cleaved crystals from them are sizeable and flat in large area.

The crystal structure was examined by XRD measurement with incident ray along the c-axis of the single crystal. Some typical diffraction patterns are shown in Figure 2. All peaks are along $(00l)$ with a narrow full-width-at-half-maximum (FWHM) around 0.1°, which shows high crystalline quality and c-axis orientation in our samples. The c

lattice parameters deduced from these patterns are about 24.61 Å, 24.24 Å and 24.03 Å for x= 0.20, 0.60 and 0.90, respectively. The small variation of c-axis for different La doping level reveals the ionic substitution effects in the out-of-plane.

### 3.2. Hole concentration and Superconductivity

The superconductivity of the crystals was characterized by the measurements of AC susceptibility. The La-Bi2201 system is so sensitive to a low magnetic field that the superconducting transition could be suppressed by a tiny DC field as low as 1 G. Figure 3(b) shows that the superconductivity is suppressed quickly under low external DC fields. In order to obtain the exact magnitude of T_c under zero external DC field, the residual field in the external superconducting coils should eliminated completely before the measurements. In our experiments, the external persistent DC field is lower than 0.5 G, and the results are more reliable and repeatable. Because of the high anisotropy and inhomogeneity in Bi2201 systems and segregation during the growth, the superconducting transition is broad for the as-grown crystals. The T_c also has a broad distribution among different crystals cleaved from the same ingot. However, after post-annealing in flowing oxygen for more than 150 hours, the superconducting transition gets much sharper, and the T_c among the samples with the same nominal composition is almost the same. Figure 3(a) shows the typical AC susceptibility data for the samples annealed at 600 ^{o}C with x=0.05, 0.10, 0.20, 0.40, 0.60 and 0.80. The T_c was defined as the point where the real part deviates from the flattened normal state part. The narrow transition width is about $1 \sim 2$ K for the annealed samples from overdoped regime to underdoped regime, which also indicates the high quality of our samples over the whole superconducting dome.

According to previous works, the superconducting dome in the phase diagram of Bi2201 is narrower than the "universal bell shape" shown as $T_c/T_{cmax} = 1 - 82.6(p - 0.16)^2$ [2]. Thus we deduced the hole concentration by using the corrected formula in Bi2201, which was proposed by Ando *et al* . in the form of $T_c/T_{cmax} = 1 - 255(p - 0.16)^2$ [17]. It should be noticed that the hole concentration p decreases as the La doping level x increases, thus the substitution of Sr^{2+} with La^{3+} enhances the electron doping and reduces the hole concentration [16]. It is found that the hole concentration p for the samples annealed at 600 ^{o}C had a linear relation with La doping level x [black line in Figure 4(a)], which is consistent with the previous work [17]. The hole concentration locates on the superconducting dome, ranging from heavily overdoped regime to extremely underdoped side where the superconductivity is absent [red line in Figure 4(b)]. In addition, the hole concentration shown in Figure 4 for our Bi-Bi2201 samples is deduced from ARPES measurements by integrating the whole Fermi surface area after a tight-binding fitting to the raw data [18]. The data in the heavily overdoped regime could not be given for the unavailable samples. For the overdoped sample above p=0.18, the nominal content of Bi for Bi-Bi2201 is less than Sr, which means Bi:Sr<1 (or x <0). For our experiments, those samples with x=0 are very tiny as needle,
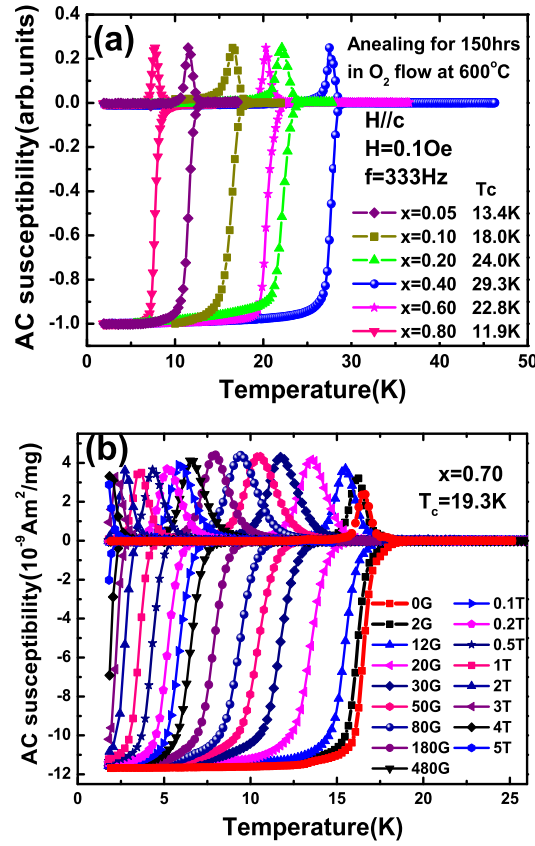
Figure 3. (color online) (a). The normalized AC susceptibility for the annealed single crystals with $x=$ 0.05, 0.10, 0.20, 0.40, 0.60 and 0.80. The T_c was defined as the point where the real part deviates from the flattened normal state part. (b). The typical AC susceptibilities under different external DC fields, which show the quick suppression of superconductivity under low DC fields.

and it could not take ARPES measurements on them. Moreover, it seems impossible to grow sizeable crystals with Bi:Sr<1 by the floating-zone method [11, 12, 14, 15]. Anyway, just like our expectations, the curve of p vs x for Bi-Bi2201 exhibits almost a straight line correlation [blue line in Figure 4(a)]. However, the slopes of the two lines are different. Because the strength of A-site disorders is the weakest in La-Bi2201 system and strongest in Bi-Bi2201 system among Bi2201 family, the T_c is suppressed more quickly by more substitutions on Sr^{2+} sites in the latter. This can be seen clearly in Figure 4(b), where a distorted dome with a narrower shape shows up in Bi-Bi2201 system [black line in Figure 4(b)]. It should be noted that we use the nominal doping content of La (the value of x) in the starting material to represent the composition of our crystals throughout this paper. Actually, the segregation always happens for the crystals grown from melt, particularly in Bi-2201 systems. We then became aware that the content of La in the single crystals may be quite different from the initial doped concentration in the polycrystalline powder. So we carried out the EDX measurements on each crystal with different doping of La, and obtained the relative percentage for each
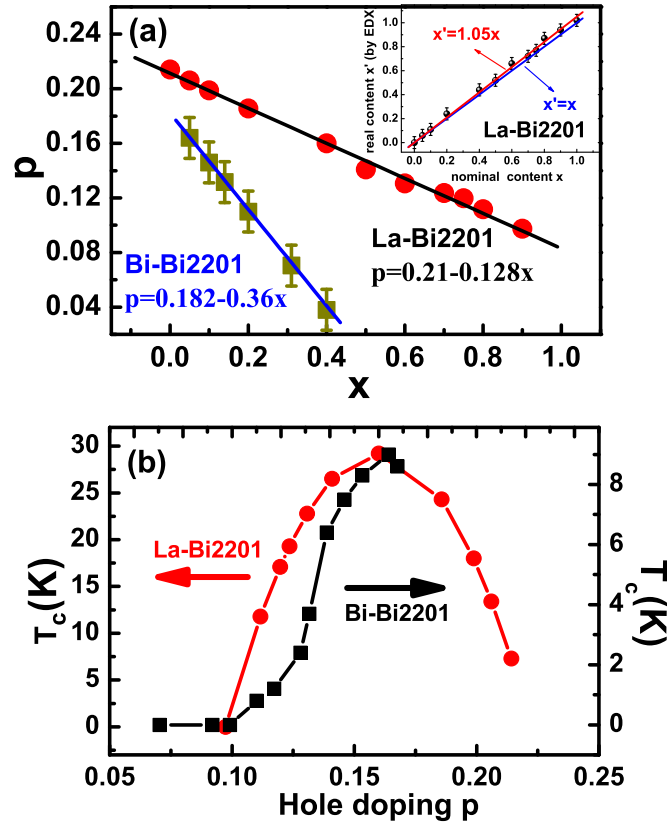
Figure 4. (color online)(a). The linear relation between hole concentration p and Ln doping level x. The solid lines are linear fitting for the scattering points. Inset: the real content doping of La for La-Bi2201, which is determined by EDX measurements. The crystal composition is very close to the starting material, where the segregation coefficient $K = C_s/C_i$ is only about 1.05, slightly above 1. (b). The superconducting dome for Bi and La doped Bi2201, where the hole concentration is deduced from the linear formulas in Figure 4(a). It can be seen that the "bell shape" is distorted in Bi-Bi2201.

element in approximate value. Based on the assumption that the proportion of Sr:La in the crystals equates to $(2-x')$:x', the real doping level of La x' is deduced and shown in the inset of Figure 4(a). It can be found that the real content of La x' is slightly larger than the nominal content x with the relation $x' = 1.05x$. Thus the crystal composition is very close to the starting material, where the segregation coefficient $K = C_s/C_i$ is only about 1.05, slightly above 1. So it is reasonable that we use the nominal values of La to represent the real contents just for convenience.

3.3. Post-annealing effects on superconductivity

In order to investigate the connection between the superconductivity and oxygen content, post-annealing experiments were carried out on our single crystals. For each nominal composition with different La doping level x, a typical as-grown single crystal was selected and then annealed at different temperatures. All treatments were made
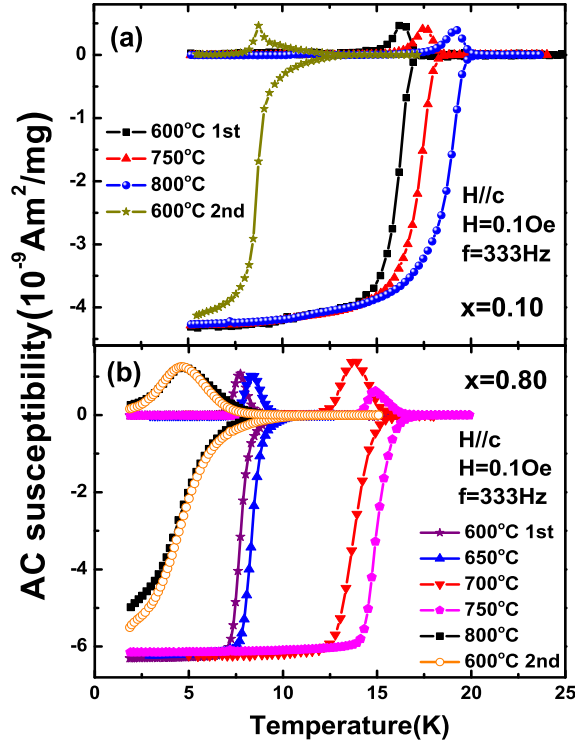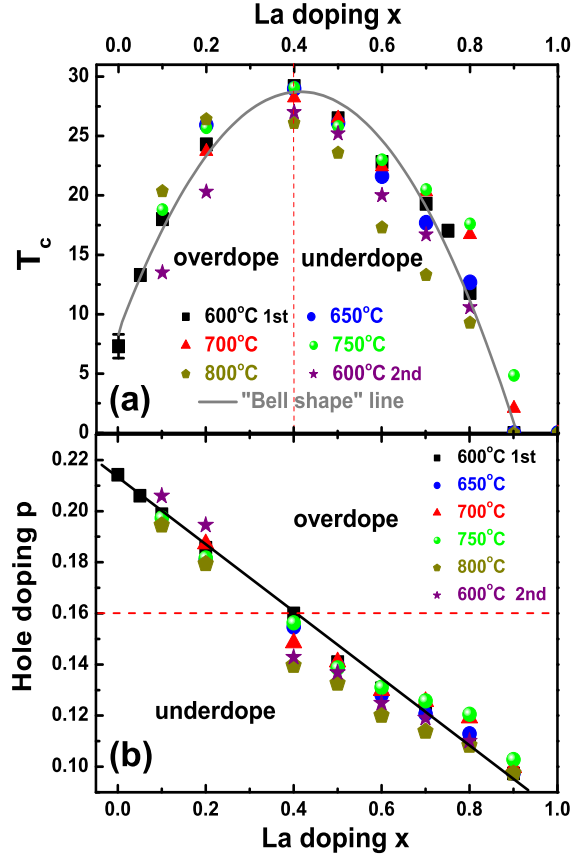
Figure 5. (color online) Typical post-annealing effects in the sample with $x=0.10$ (overdoped) and $x=0.80$ (underdoped) .

under 1 atm oxygen pressure with flowing rate $30 \sim 50$ cc/min for more than 150 hours. It was found that the oxygen distribution in the crystal with moderate size reached the equilibrium state after annealing for more than 100 hours, because the superconducting transition and T_c could not be changed any more even annealing for more time at the same temperature. So 150 hours for each step of post-annealing are enough. At the end of the treatment, the samples were quenched to room temperature in air, and then the AC susceptibility was measured on them. Several post-annealing temperatures were chosen, changing from $600\,^oC$ to $800\,^oC$ at $50\,^oC$ per step. As a final check of reversibility, all samples were annealed at $600\,^oC$ again at the final step. We used the same sample for each nominal doping level of La throughout the whole procedure.

Figure 5 shows the post-annealing effects on the samples with $x=0.10$ and 0.80. Apparently, the superconductivity could be tuned by post-annealing. For the sample with $x=0.10$, the T_c increases as the post-annealing temperature increases. In the final step of post-annealing at $600\,^oC$, the superconducting transition could not return to the shape as that in the first step. There is a long tail above the sharp peak of the imaginary part of AC susceptibility, which indicates that the crystal becomes much inhomogeneous in the oxygen distribution. The as-grown crystals with $x=0.80$ exhibit no superconductivity above 1.6 K. However, after post-annealing at $600\,^oC$ for the first step, superconductivity with $T_c=11.9$ K emerges, and it can be promoted by post-annealing at higher temperature $650\,^oC \sim 750\,^oC$. The superconducting transition

Figure 6. (color online) The post-annealing effects on T_c and p at different temperatures for each La doping level x in La-Bi2201 system.

width and the magnitude of diamagnetic signal only change a little during these steps. Unfortunately, after post-annealing at 800 °C, T_c drops down for several Kelvins and the superconducting transition gets much broader. Although the sample was annealed again at 600 °C at the last step, the transition and T_c can not be improved much more. This is similar to the Bi doped Bi2201 system. It seems not easy to tune the T_c of Bi-Bi2201 by post-annealing [19, 20, 21]. According to our previous work, the Bi-Bi2201 system has no significant post-annealing effects at any temperatures less than 600 °C, while annealed at higher temperatures makes the crystals melting down [14].

The post-annealing effects on T_c are summarized in Figure 6(a) for each doping in La-Bi2201 system. Obviously, the magnitude of T_c varies as the post-annealing temperature changes, and the detailed behaviors are also various for different La doping levels. For the optimal doping samples with $x= 0.40$, T_c is very robust under most post-annealing cases. However, in the heavily underdoped regime with $x \geq 0.70$, T_c is affected easily by post-annealing. The T_c reaches the maximum magnitude after post-annealing at 750 °C in the underdoped regime. While in the overdoped regime, the highest T_c could be obtained by post-annealing at 800 °C. Unfortunately, the result of post-annealing at 800 °C is anomalous for all underdoped samples, which gives a much lower T_c and a broader transition. The "bell shape" is distorted in the case of post-

annealing at 800 ^{o}C, too. Moreover, after post-annealing at 600 ^{o}C again at the final step, the T_c can not return to the magnitude at the first step. This suggests that the crystal structure may distort at such high temperatures being close to its melting point. It is more serious in the overdoped regime, since the melting points for these samples are lower than those in the underdoped side. The T_c after post-annealing at 600 ^{o}C for the final step drops to much lower level, and the long-tail feature in AC susceptibility is also very clear. Furthermore, if we plot the hole concentration p for each T_c in the same La doping level, it could be found that the hole concentration related to the oxygen content also varies with different post-annealing temperature [Figure 6(b)], where p is determined by the formula from Ando *et al* . [17] using $T_{cmax} = 29.2$ K. For the first step of post-annealing at 600 ^{o}C, the relation between p and x is almost linear. It is also deviated seriously in the case of post-annealing at 800 ^{o}C. After the second step of post-annealing at 600 ^{o}C, the hole concentration p could not return to the same level as the first step of post-annealing at 600 ^{o}C. It increases in the overdoped regime, while the case is opposite in the underdoped regime. These different effects of post-annealing suggest that the nature of superconducting mechanism in the overdoped regime may not be the same as the underdoped regime [1]. One typical example is that the phase separation may exist in the overdoped regime [22], where it is absent in the underdoped regime [23, 24].

4. Summary

In summary, we have successfully grown high-quality $Bi_2Sr_{2-x}La_xCuO_{6+\delta}$ ($0{\leq}x{\leq}1.00$) single crystals by TSFZ method. The sharp peaks in the patterns of XRD indicate high crystalline quality for our samples. After post-annealing in the flowing oxygen at 600 ^{o}C, The results of AC susceptibility show sharp superconducting transitions. The hole concentration p exhibits a linear relation with La doping level x. It ranges from the heavily overdoped regime ($p \approx 0.2$) to the extremely underdoped side ($p \approx 0.08$) where the superconductivity is absent. Comparing between the La-Bi2201 and Bi-Bi2201 system, the superconducting dome has a narrower shape in the latter due to the stronger effects from A-site disorders. The hole concentration could also be tuned by post-annealing at different temperatures in flowing oxygen. The effects of post-annealing on T_c and p are summarized over the whole superconducting regime of the phase diagram, which indicate the nature of superconductivity in overdoped regime may be different from that in underdoped regime.

References

[1] Lee P A, Nagaosa N and Wen X G 2006 *Rev. Mod. Phys.* **78** 17

[2] Presland M R, Tallon J L, Buckley R, Liu R S and Flower N 1991 *Physcica* C **176** 95

[3] Eisaki H, Kaneko N, Feng D L, Damascelli A, Mang P K, Shen K M, Shen Z X and Greven M 2004 *Phys. Rev.* B **69** 064512

[4] Fujita K, Noda T, Kojima K M, Eisaki H and Uchida S 2005 *Phys. Rev. Lett.* **95** 097006

[5] Okada Y, Takeuchi T, Baba T, Shin S, Ikuta H 2008 *J. Phys. Soc. Jpn.* **77** 074714

[6] Slezak J A *et al* 2008 *PNAS* **105** 3203

[7] Michel C, Hervieu M, Borel M M, Grandin A, Deslandes F, Provost J and Raveau B 1987 *Z. Phys.* B **68** 421

[8] Fleming R M, Sunshine S A, Schneemeyer L F, Van Dover R B, Cava R J, Marsh P M, Waszczak J V, Glarum S H, Zahurak S M and DiSalvo F J 1990 *Physcica* C **173** 37

[9] Martovitsky V P, Gorina J I, and Kaljushnaia G A 1995 *Solid State Commun.* **96** 893

[10] Gorina Y I, Kalyuzhnaya G A, Rodin V V, Sentyurina N N, Stepanov V A and Chernook S G 2007 *Crystallography Reports* **52(4)** 735

[11] Liang B, Maljuk A and Lin C T 2001 *Physcica* C **361** 156

[12] Liang B and Lin C T 2004 *J. Crystal Growth* **267** 510

[13] Ando Y and Murayama T 1999 *Phys. Rev.* B **60** R6991

[14] Luo H Q, Fang L, Mu G and Wen H H 2007 *J. Crystal Growth* **305** 222

[15] Lin C T, Freiberg M, Schönherr E 2000 *Physcica* C **337** 270

[16] Ono S and Ando Y 2003 *Phys. Rev.* B **67** 104512

[17] Ando Y, Hanaki Y, Ono S, Murayama T, Segawa K, Miyamoto N and Komiya S 2000 *Phys. Rev.* B **61** R14956

[18] Pan Z H *et al* pre-print on Arxiv: 0806.1177

[19] Vedeneev S I, Jansen A G M, Haanappel E and Wyder P 1999 *Phys. Rev.* B **60** 12467

[20] Vedeneev S I and Maude D K 2004 *Phys. Rev.* B **70** 184524

[21] Sonder F, Chakoumakos B and Sales B 1989 *Phys. Rev.* B **40** 6872

[22] Uemura Y J *et al.* 1993 *Nature* **364** 605

[23] Wen H H, Yang W L, Zhao Z X and Ni Y M 1999 *Phys. Rev. Lett.* **82** 410

[24] Wen H H 2000 *PNAS* **97** 11145